Evolution, 2026, **80**(**7**), 1452–1466
https://doi.org/10.1093/evolut/qpag069
Advance access publication 24 April 2026
Original Article

Geographic isolation after admixture generates a distinct lineage in an Atlantic Forest bird

Rafael D. Lima [1,2], Fernanda Bocalini[1], Vitor Gomes[1], Emily N. Ostrow [3], Therese A. Catanach[3], Jason D. Weckstein [3,4], Luís Fábio Silveira[1], Vítor Q. Piacentini[5]

[1]Museu de Zoologia da Universidade de São Paulo, São Paulo, SP, Brazil
[2]Department of Biological Sciences, University of Texas at El Paso, El Paso, TX, United States
[3]Department of Ornithology, Academy of Natural Sciences of Drexel University, Philadelphia, PA, United States
[4]Department of Biodiversity, Earth, and Environmental Science, Drexel University, Philadelphia, PA, United States
[5]Departamento de Biologia e Zoologia & Programa de Pós-graduação em Zoologia, Instituto de Biociências, Universidade Federal de Mato Grosso, Cuiabá, MT, Brazil

Corresponding author: Department of Biological Sciences, University of Texas at El Paso, El Paso, TX 79902. Email: rafael-dlima@hotmail.com

Abstract

Although traditionally viewed as opposing divergence, hybridization can have diverse evolutionary outcomes. Yet, its role in lineage divergence remains unclear. To investigate this process, we examined the evolutionary history of the Black-cheeked Gnateater (*Conopophaga melanops*) from the Atlantic Forest of eastern Brazil. The central subspecies, *C. m. perspicillata*, exhibits plumage traits intermediate to northern and southern populations, raising the question of whether this pattern reflects isolation-by-distance, recent hybridization, or past admixture. Using genome-wide markers from sequencing of ultraconserved elements along with phenotypic data, we assessed genetic structure and trait variation across the species' range. Our analyses reveal four population genetic clusters, with central populations exhibiting clear signatures of historical admixture. Despite this admixture, central populations are genetically differentiated from northern and southern lineages and sing a distinct song, suggesting divergence following admixture or transgressive segregation. We propose that past hybridization followed by geographic isolation contributed to the formation of a divergent, reticulate lineage within the Black-cheeked Gnateater. This system provides an opportunity to investigate how gene flow and allopatric divergence interact to shape lineage diversity and offers a natural framework for testing the conditions under which reticulate lineages may emerge, persist, and diverge.

Keywords: divergence with gene flow, historical DNA, introgression, refugia, speciation, suboscine

Introduction

Hybridization is common across animals and contributes to diverse evolutionary outcomes (Abbott et al., 2013; Taylor & Larson, 2019). Introgressive hybridization may slow or reverse differentiation between populations, ultimately leading to lineage fusion (Kearns et al., 2018; Taylor et al., 2006). Yet, introgression can also introduce novel genetic and phenotypic variation that supports lineage persistence or promote the emergence of new lineages (Edelman & Mallet, 2021; Peñalba et al., 2024; Seehausen, 2004). In all cases, gene flow contributes to reticulate evolution, producing lineages with admixed genotypes whose histories are better represented by networks than bifurcating phylogenetic trees (Mallet et al., 2016).

Genomic data increasingly reveal that reticulate evolution is far more common than once assumed (Mallet et al., 2016). Importantly, reticulation may result from a wide variety of geographic and demographic scenarios. In many cases, phylogenetic reticulation can reflect episodic gene flow during lineage divergence (Cui et al., 2013; Musher et al., 2022; Singhal et al., 2021). In others, lineages with admixed ancestry may reflect lineage fusion events (Garrick et al., 2014; Kearns et al., 2018), historical hybridization (McCallum et al., 2024; Taylor et al., 2021; Weckstein et al., 2001), past introgression from extinct lineages (Barlow et al., 2018; Kuhlwilm et al., 2019), or hybrid lineage formation (Bertola et al., 2024; Brelsford et al., 2011; Lopes et al., 2023; Wu et al., 2023). Despite accumulating examples, the processes by which admixed lineages persist, diverge, or become reproductively isolated remain poorly understood. Systems where hybridization and geographic isolation have occurred recently offer valuable opportunities to investigate the conditions under which reticulate histories form.

The Black-cheeked Gnateater (*Conopophaga melanops*) is a promising avian system for studying these dynamics. Endemic to the Atlantic Forest of eastern Brazil, this species inhabits the understory of lowland humid forests, a landscape historically shaped by the expansion and contraction of forest refugia during Pleistocene climatic oscillations and bisected by major river systems that act as barriers to gene flow (Carnaval & Moritz, 2008; Peres et al., 2020). *Conopophaga* gnateaters are generally highly sedentary and philopatric (Greeney, 2018; Whitney, 2003), traits that limit dispersal and facilitate population structuring across such barriers. The species comprises three currently allopatric subspecies described based on plumage differences

Received June 18, 2025; revisions received March 30, 2026; accepted April 21, 2026
Associate Editor: Scott Taylor; Handling Editor: Jason Wolf

distributed along a north–south axis (Greeney, 2018). The northernmost subspecies, *C. m. nigrifrons*, has a wide black forehead band, white breast, and grayish back in males, and a grayish crown in females. In the southernmost subspecies, *C. m. melanops*, males typically exhibit a narrow or absent black forehead band, a gray breast, and a brown back, and females have a relatively brighter orange–brown crown. The central subspecies, *C. m. perspicillata*, exhibits somewhat intermediate plumage traits (Figure 1; Greeney, 2018; Whitney, 2003). This gradual geographic transition in plumage from north to south could reflect several alternative evolutionary scenarios, including (1) isolation-by-distance, (2) recent hybridization between formerly isolated lineages, or (3) the persistence of a distinct reticulate lineage formed via past hybridization. Another possibility, divergence with ongoing gene flow, could also generate this pattern provided that there is sufficiently strong divergent selection to counterbalance gene flow (Feder et al., 2012). However, the subspecies are currently allopatric and the environments they occupy do not appear to differ noticeably (Greeney, 2018).

Distinguishing among these alternative scenarios requires evaluating the extent and structure of genotypic and phenotypic variation across the species' range. A pattern of gradual genomic and phenotypic change without discrete population boundaries would support isolation-by-distance. In contrast, evidence of recent-generation hybrids and a spatially well-defined admixture zone would suggest recent secondary contact between historically isolated northern and southern lineages. Finally, if individuals in the central range show no signs of recent hybridization but have consistent genomic contributions from the northern and southern subspecies, along with reduced gene flow into neighboring populations, this would support the persistence in allopatry of an admixed lineage formed through past hybridization.

Previous genetic work based on few loci documented discrete population structure aligned with the three plumage-based subspecies (Batalha-Filho et al., 2014; Cabanne et al., 2016). However, limited genetic sampling often masks reticulation, as shown by early studies of other birds that inferred simple bifurcating histories (Ribas et al., 2018; Schultz et al., 2019; Thom & Aleixo, 2015) later overturned by genomic data revealing extensive reticulation (Del-Rio et al., 2022; Musher et al., 2022, 2024; Pulido-Santacruz et al., 2020). This raises the possibility that the Black-cheeked Gnateater also harbors a more complex evolutionary history consistent with its clinal plumage variation. Lastly, geographic variation in other key traits remains unexplored. Because variation in bird vocalizations often promotes premating reproductive barriers (Price, 2008; Uy et al., 2018), vocal divergence might provide a strong indicator of reproductive barriers among Black-cheeked Gnateater populations.

To discriminate among alternative divergence and admixture scenarios, we integrate genomic, plumage, and vocal data across the species' range. First, we analyze genome-wide SNP data and a mitochondrial gene from 45 individuals spanning the full range of the Black-cheeked Gnateater to characterize population structure and admixture. We then apply phylogenetic tree and network methods to characterize phylogenetic discordance and reticulation, and we examine geographic patterns of heterozygosity to distinguish between different hybrid classes. Finally, we analyze spatial patterns in plumage and vocal traits to compare phenotypic and genetic structure and assess the distinctiveness of the central subspecies. These combined analyses allow us to evaluate whether variation in the Black-cheeked Gnateater is best explained by isolation-by-distance, recent hybridization, or the persistence of an admixed lineage formed through past hybridization.

Methods

Genetic sampling, DNA extraction, and sequencing

We generated genome-wide SNP data for 45 individuals from 31 localities across the Black-cheeked Gnateater's range (Figure 1A). These included 14 individuals of *C. m. melanops*, 18 of *C. m. perspicillata*, and 13 of *C. m. nigrifrons* (Supplementary Table S1). For phylogenetic analyses, we also sequenced four Black-bellied Gnateaters (*C. melanogaster*) to use as outgroups. Samples were obtained during our own field work and from existing collections (details in Supplementary Table S1). For 31 fresh tissue samples, we extracted genomic DNA using standard extraction kits (Qiagen DNeasy Blood & Tissue Kit and Invitrogen PureLink Genomic DNA Mini Kit) following the manufacturers' instructions. To fill in important geographic sampling gaps where fresh tissue samples were not available, we also extracted historical DNA from 10 toepads sampled from museum study skins using a silica spin-column protocol adapted from Harvey et al. (2020). These historical DNA extractions were performed with dedicated equipment to prevent cross-contamination. Given the mix of high-quality and highly degraded DNA in our dataset, we selected ultraconserved elements (UCEs) for genomic sequencing. We sent DNA extracts to Rapid Genomics (Gainesville, FL, USA) for library preparation, enrichment, and sequence capture using either the Tetrapod UCE 2.5K or 5K probe sets (details in Supplementary Table S1), following a protocol modified from Faircloth et al. (2012). To ensure consistent coverage across samples, we restricted all downstream analyses to the set of loci shared by both probe sets (~2,500 loci).

Genetic data processing

We obtained an average of 2,332,907 read pairs per sample. We used Illumiprocessor v.2.1 (Faircloth, 2013) and Trimmomatic v.0.39 (Bolger et al., 2014) within Phyluce v.1.7.2 (Faircloth, 2016) to remove adapters, barcodes, and low-quality regions from the raw reads. We then used SPAdes v.3.14.1 (Prjibelski et al., 2020) to assemble the cleaned reads into contigs and Phyluce v.1.7.2 (Faircloth, 2016) to match the assembled contigs to the probe set. This process successfully assembled an average of 3,417 contigs per sample, with a mean coverage of 26×. Tissue samples sequenced with the 2.5K probe set yielded an average of 2,108 contigs (SD = 15), whereas those sequenced with the 5K probe set yielded 4,459 contigs on average (SD = 13). Toepad samples, sequenced with the 5K probe set, yielded an average of 3,807 contigs (SD = 583). Mean contig length was 774 bp for tissue samples (SD = 87) and 430 bp for toepad samples (SD = 173).

We selected the sample with the greatest number of assembled UCE loci (tissue MZUSP 91,214) as a pseudo-reference for mapping and calling SNPs for all samples, using a custom script modified from Harvey et al. (2016). Briefly,

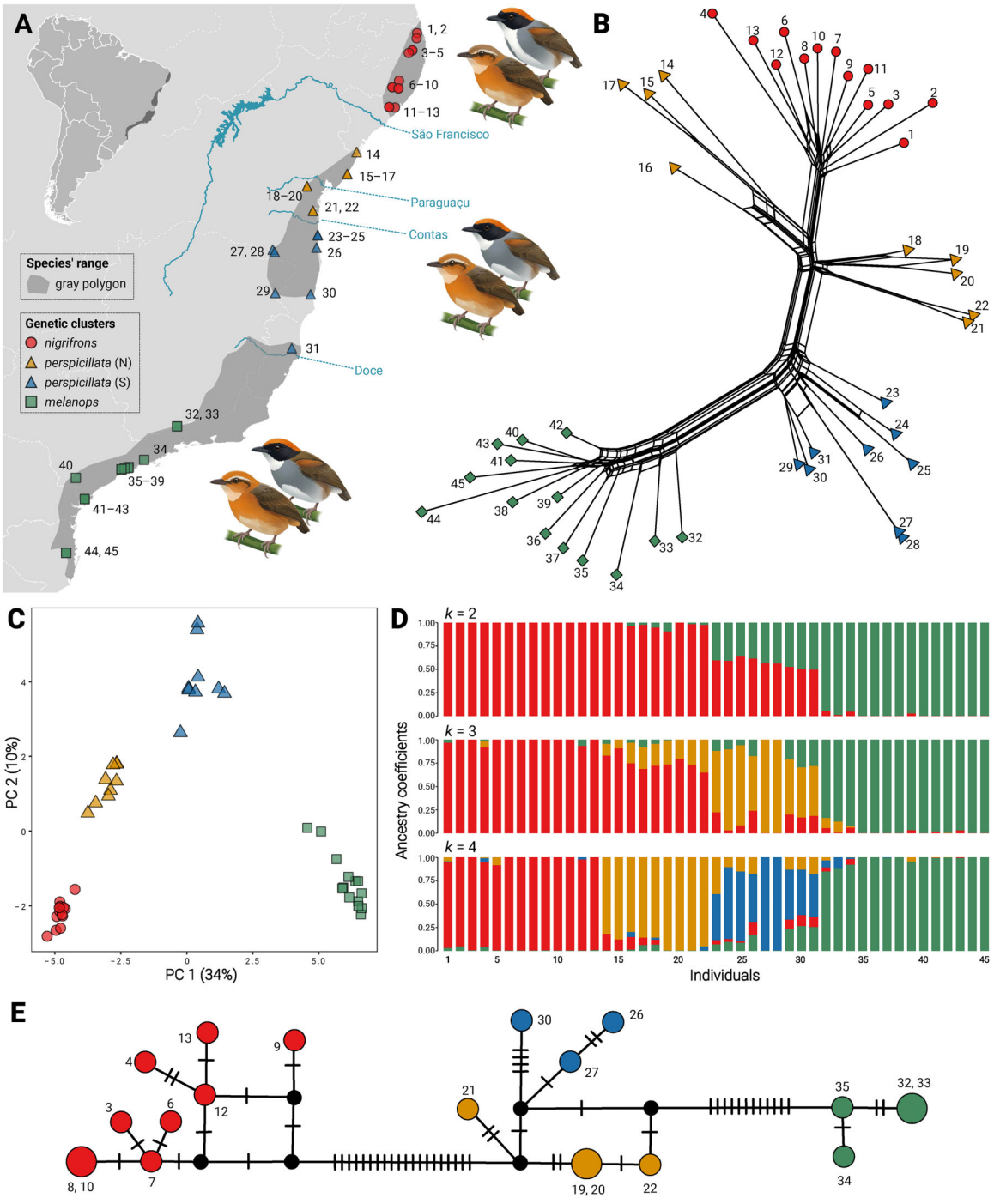

Figure 1. Population genetic structure of the Black-cheeked Gnateater. (A) Circles, triangles, and squares on the main map indicate sampling locations of genotyped individuals. Sample numbers are the same across panels. The dark gray polygons on the maps illustrate the species' range, adapted from Greeney (2018). Rivers referenced in the text are labeled on the main map. Inset map shows the species' range within South America. Bird illustrations show the main plumage differences among subspecies (details in Introduction). (B) Distance-based phylogenetic network showing relatedness among samples and reticulation among population clusters, based on 758 genome-wide single nucleotide polymorphisms (SNPs). (C) Principal component analyses (PCA) depicting population clustering on two principal component axes that together explained 44% of the genotypic variance in the dataset with 758 genome-wide SNPs. (D) sNMF analyses showing genetic admixture among populations across three clustering scenarios, based on 553 unlinked SNPs. (E) Haplotype network of mitochondrial ND2 sequences. This network contains 20 of the 45 individuals in the nuclear genetic analyses. Numbers identify samples in each haplotype. Circle size is proportional to haplotype frequency: smaller circles denote haplotypes found in only one sample, and larger circles those found in two samples. Inferred intermediate haplotypes are shown as black circles on branches connecting observed haplotypes. Tick marks between haplotypes represent mutation steps.

we used BWA v.0.7.17 (Li & Durbin, 2010), SAMtools v.1.11 (Li et al., 2009), and GATK v.3.8 (McKenna et al., 2010) to index the reference contigs, aligned trimmed raw reads to the reference, called SNPs and indels, and obtained phased alleles. This process yielded a dataset of 155,803 SNPs in variant call format.

We then applied various filters to this SNP dataset using the R packages *vcfR* (Knaus & Grünwald, 2017) and *SNPfiltR* (DeRaad, 2022) to prepare optimized SNP datasets for analysis. We first removed SNPs with quality scores <30 and read depth <5, those with more than two alleles, those falling outside of a 0.25–0.75 allele balance range, and those with a mean depth of coverage >150, resulting in a dataset of 41,912 high-quality SNPs with 61% overall missing data. Then, we iteratively explored the impact of missing data and minor allele frequency thresholds (Linck & Battey, 2019; Willing et al., 2012; Yi & Latch, 2022) on our analyses. First, we used the *SNPfiltR* function *assess_missing_data_pca* to examine sample clustering across six per-SNP completeness thresholds, ranging from 75% to 99%, to ensure that missing data were not driving patterns of sample clustering. Based on this exploratory analysis, we applied a per-SNP completeness cutoff of 95%, which eliminated missing data effects. Subsequently, we conducted exploratory PCA and calculated measures of genetic differentiation (Weir and Cockerham's F_{ST} and Nei's D) across various minor allele count (MAC) cutoffs, ranging from 1 to 15, to assess their impact on inferences of population differentiation. We observed that removing rare alleles did not change clustering patterns but gradually increased the proportion of variance explained in the first principal component axes, indicating that the primary signals of differentiation in our dataset are associated with common alleles. However, removing rare alleles also resulted in a gradual increase in F_{ST} and Nei's D estimates, as the more filtered datasets contained increasingly higher proportions of loci with significant population differentiation. Since focusing on common alleles with high differentiation could lead to an overestimation of genetic differentiation (Willing et al., 2012), we applied conservative a MAC cutoff of 2 to only remove rare alleles that might result from sequencing error.

Finally, we exported three optimized SNP datasets for downstream analyses. For population genetic analyses, we exported a "linked SNP dataset" comprising 758 SNPs and an "unlinked SNP dataset" of 553 SNPs with one randomly selected SNP per 10,000 bp, designed for use in analyses that require unlinked loci. Both datasets included the 45 Black-cheeked Gnateater individuals and had 2% overall missing data. For phylogenetic analysis, we exported an unlinked dataset with 828 SNPs shared by all Black-cheeked Gnateater individuals and the outgroup samples. This dataset also had 2% overall missing data.

To examine mitochondrial variation, we used MITObim v.1.9.1 (Hahn et al., 2013) to assemble draft mitochondrial genomes from off-target UCE reads, and used GENEIOUS v.9.1.8 (Kearse et al., 2012) to manually extract the NADH dehydrogenase subunit 2 (ND2) gene from these assemblies. We then exported a trimmed alignment with the 20 highest-quality sequences (each 1030 bp in length) for further analysis.

Phylogenetic inference

To assess patterns of phylogenetic discordance and test for signals of reticulate evolution, we performed both tree- and network-based phylogenetic analyses. First, we used SNAPP (Bryant et al., 2012), implemented in BEAST2 v.2.4.8 (Bouckaert et al., 2014), to infer a species tree from the set of 828 SNPs, with outgroup samples included and ingroup sampling localities as tips. To meet the algorithm's assumption of no gene flow between lineages, we excluded individuals with more than 40% admixture (as measured by sNMF; see below). We used default priors and conducted two independent runs of 5 million generations each, sampling every 1,000 steps and discarding the first 10% as burn-in. Effective sample sizes >400 were confirmed in Tracer 1.7.1 (Rambaut et al., 2018). We generated maximum clade credibility trees using LogCombiner and TreeAnnotator (Bouckaert et al., 2014) and visualized them with DensiTree v.2.2.6 (Bouckaert & Heled, 2014).

We also used BEAST2 v.2.4.6 (Bouckaert et al., 2014) to infer a time-calibrated gene tree from the mitochondrial ND2 alignment. We determined the best nucleotide substitution model (TIM3 + I) using the corrected Akaike Information Criterion (AICc; Hurvich & Tsai, 1989) in jModelTest2 (Darriba et al., 2012). Following Nabholz et al. (2016), we applied a body-mass correction using a mass of 20.1 g (Whitney, 2003) to estimate an average substitution rate of 0.0186 substitutions per site per million years. The analysis used a relaxed molecular clock, a coalescent constant-population prior, no topological constraints, and a randomly generated starting tree. We ran Markov Chain Monte Carlo analyses for 500 million generations, sampling every 1,000 steps, and assessed convergence across independent runs by confirming effective sample sizes >400 in TRACER v.1.7.1 (Rambaut et al., 2018). After discarding the first 10% of samples as burn-in, we summarized results as a maximum clade credibility tree in TreeAnnotator v.2.4.4 (Bouckaert et al., 2014), retaining nodes with posterior probabilities ≥0.5.

Since a bifurcating phylogenetic tree may not accurately represent the evolutionary history of the Black-cheeked Gnateater, we also constructed an unrooted phylogenetic network to visualize evolutionary relationships while accounting for possible reticulation (Huson & Bryant, 2006). We first calculated a matrix of pairwise genetic distances (*sensu* Nei, 1972) between samples in the linked SNP dataset, using the *stamppNeisD* function from the R package *StAMPP* (Pembleton et al., 2013). This distance matrix was then used to build a network with the neighbor-net algorithm (Bryant & Huson, 2023) in SplitsTree v.4.19.2 (Huson & Bryant, 2006). Finally, we visualized the network using the R packages *phangorn* (Schliep, 2011), *ggtree* (Yu et al., 2017), and *tanggle* (Schliep et al., 2017).

Population genetic structure

We conducted three complementary analyses to estimate population structure from nuclear genome-wide SNP data. First, we performed a PCA using the function *dudi.pca* from the R package *adegenet* v.2.1.10 (Jombart, 2008) to visually assess genetic structure without prior assumptions about population assignment or the number of clusters. To statistically validate our qualitative assessment of genetic struc-

ture based on the PCA, we applied two distinct clustering algorithms. First, we applied the *K*-means clustering algorithm via the *adegenet* function *find.clusters* (Jombart, 2008) to determine the statistically optimal number of clusters (k) in the linked SNP dataset. We retained all principal components summarizing the genotypic variance in the dimension-reduction step and performed 100 replicate runs of the *K*-means clustering algorithm, considering a range of $k = 1$–10. The best fitting k was selected based on the smallest Bayesian information criterion (BIC) value. After determining the statistically optimal k, we performed a discriminant analysis of principal components (DAPC; Jombart et al., 2010) using the *adegenet* function *dapc* to examine the separation among the identified clusters, retaining $k - 1$ principal components following Thia (2023). Second, we used sparse nonnegative matrix factorization (sNMF; Frichot et al., 2014) as implemented in the R package *LEA* (Frichot & François, 2015) as an alternative clustering algorithm. Unlike *K*-means, sNMF can assign samples to multiple clusters if they are admixed. We performed 100 replicate runs of the sNMF algorithm, considering values of k ranging from 1 to 10 and four different values of the α regularization parameter (10,100, 500, and 1,000), using the unlinked SNP dataset as input. The statistically optimal k and α were selected based on the smallest cross-entropy values, with the final results taken from the replicate with the lowest cross-entropy.

To measure the magnitude of genetic differentiation among genetic clusters identified in the previous analyses, we calculated pairwise F_{ST} (*sensu* Weir & Cockerham, 1984) with the function *stamppFst* from the R package *StAMPP* (Pembleton et al., 2013) and measured the number of fixed SNPs between clusters using a custom R script. Both analyses used the linked SNP dataset as input.

To further explore population structure, we also inferred an estimated effective migration surface (EEMS; Petkova et al., 2016). We used the unlinked SNP dataset to calculate a pairwise genetic dissimilarity matrix that we used as input to perform three replicate runs of EEMS with 20 million MCMC iterations each, discarding the first 1 million iterations as burn-in in each run. We ran EEMS using deme sizes ranging from 200 to 600 and retained results with deme size equal to 400 after exploring parameter space. To test whether patterns of genetic variation in the Black-cheeked Gnateater are consistent with isolation-by-distance, we used Spearman's correlation and polynomial regression to assess the relationship between geographic and genetic distances as calculated in the EEMS.

To assess mitochondrial genetic differentiation without assuming a bifurcating history, we also used the ND2 alignment to construct a TCS haplotype network (Clement et al., 2000) with PopART v.1.7 (Leigh & Bryant, 2015) and to calculate uncorrected pairwise distances between populations with a custom R script.

Genetic admixture

To assess genetic admixture among populations, we estimated individual ancestry coefficients using sNMF (Frichot et al., 2014) in the R package *LEA* (Frichot & François, 2015). We examined admixture under three alternative clustering scenarios ($k = 2$–4), using the same parameters described above for identifying the statistically optimal k in sNMF. To distinguish between historical and contemporary gene flow, we employed triangle plots to classify admixed individuals by hybrid class. These plots show interclass heterozygosity (i.e., the proportion of loci with alleles from both parental populations) plotted against a hybrid index. The set of possible coordinates forms a triangular shape, with different positions along the triangle indicating different hybrid classes (Wiens et al., 2025). In cases of neutral admixture with ongoing gene flow, hybrids are expected to occupy a specific area of the triangle (Fitzpatrick, 2012; Wiens et al., 2025). As immigration from the parental populations ceases, hybrid populations tend to lose alleles through drift, resulting in increasing homozygosity. This leads to a decrease in interclass heterozygosity while the hybrid index remains relatively stable (Fitzpatrick, 2012), enabling distinguishing between historic and contemporary hybridization. To generate the triangle plots, we used multiple functions from the R package *triangulaR* (Wiens et al., 2025) to identify ancestry-informative SNPs between the northernmost and southernmost genomic clusters and to calculate interclass heterozygosity and hybrid indices based on these SNPs. We analyzed triangle plots using two allele frequency difference thresholds ($D = 1$ and 0.75) to evaluate their impact on hybrid class inference. Lower thresholds result in more loci and can significantly improve the precision of hybrid index and interclass heterozygosity estimates for late-generation hybrids with little loss in accuracy for F_1 hybrids (Wiens et al., 2025). Importantly, even small sets of highly differentiated SNPs (15–30 loci) are sufficient for generating reliable plots (Wiens et al., 2025). Lastly, we used a custom R script to calculate the proportion of heterozygous loci for each sample in the linked SNP dataset, and plotted heterozygosity against latitude to investigate geographic variation in heterozygosity.

Phenotypic trait data collection and geographic cline analysis

To characterize geographic variation in phenotypes and compare it to patterns of genetic variation, we gathered data on plumage and vocal traits from across the species' range. Plumage traits were scored for 33 of the 45 genotyped individuals, along with an additional 121 study skins held in the Museu de Zoologia da Universidade de São Paulo. These individuals included 104 *C. m. melanops* (67 males, 37 females), 13 *C. m. perspicillata* (7 males, 6 females), and 37 *C. m. nigrifrons* (18 males, 19 females), totaling 154 individuals (Supplementary Table S2). Four plumage traits were assessed: Female crown color was scored on a scale from 0 to 3 with "0" being orange-brown, "1" being dull brown, "2" being olive-brown, and "3" being grayish-olive. Male back color was categorized as either "0" (brown) or "1" (grayish). Male breast pattern was scored on a scale from 0 to 2 with "0" having a clearly defined gray breast band, "1" having a fuzzy gray breast band, and "2" having a white central breast. Male black forehead band width was measured in millimeters with a digital caliper to the nearest 0.1 mm. Supplementary Figure S1 illustrates each plumage trait and corresponding score. All scoring was done by a single author (VG) and under a single light source. To standardize the data, we scaled all plumage trait scores to range from 0 to 1.

To assess vocal variation in the species, we analyzed 37 songs from 25 individuals spanning 24 different lo-

calities, sourced from three publicly available archives of avian sound recordings (Macaulay Library, xeno-canto, and WikiAves). These included 23 individuals of *C. m. melanops*, 12 of *C. m. perspicillata*, and 2 of *C. m. nigrifrons* (Supplementary Table S3), none of which is included in our genetic datasets. We initially measured 10 spectral and temporal variables with default settings in RAVEN Pro v.1.6 (Charif et al., 2010), but preliminary analyses showed that geographic variation was restricted to pace (i.e., notes per second). Thus, we retained only pace for further analysis. As with plumage traits, song pace was scaled from 0 to 1.

Because the range of the Black-cheeked Gnateater spans a broad latitudinal band with minimal longitudinal range, we used latitude as the geographic axis in our geographic cline analysis. We examined clinal transitions in allele frequencies and phenotypic traits by plotting the genotypic hybrid index based on fixed alleles and phenotypic trait scores against the latitude of sampling locations.

Results

Phylogenetic inference

Coalescent-based species tree reconstruction based on genome-wide nuclear SNP data identified four well-supported clades: (1) one comprising *C. m. nigrifrons*; (2) one comprising *C. m. perspicillata* north of the Contas River; (3) one comprising *C. m. perspicillata* south of the Contas River; and (4) one comprising *C. m. melanops* (Supplementary Figure S2). *Conopophaga m. nigrifrons* was recovered as sister to the northern *C. m. perspicillata* clade with strong statistical support (posterior probability = 0.99). *Conopophaga m. melanops* grouped with the southern *C. m. perspicillata* clade, but this relationship lacked statistical support (posterior probability = 0.67). The southern *C. m. perspicillata* clade featured extensive topological discordance, with many loci placing it as sister to the northern *C. m. perspicillata* clade (Supplementary Figure S2). It is likely that this species tree topology reflects the dominant genealogical history driven by extensive nuclear gene flow (see genetic admixture results), and the placement of the southern *C. m. perspicillata* cluster is best considered unresolved given its low statistical support.

A time-calibrated gene tree based on the mitochondrial ND2 gene identified three clearly distinct and well-supported clades corresponding to the three plumage-based subspecies (Supplementary Figure S3). The *C. m. perspicillata* clade had the most structure, although samples separated by the Contas River were not reciprocally monophyletic (Supplementary Figure S3). *Conopophaga m. nigrifrons* was recovered as sister to a clade comprising the *C. m. perspicillata* and *C. m. melanops* clades with strong statistical support (posterior probability = 1). Divergence time estimates using a relaxed molecular clock and assuming constant population sizes indicated that *C. m. nigrifrons* split from the clade including *C. m. perspicillata* and *C. m. melanops* around 760,000 years ago (95% HPD: 1,030,000–510,000), and *C. m. perspicillata* and *C. m. melanops* split around 442,300 years ago (95% HPD: 630,000–270,000).

A distance-based phylogenetic network inferred from nuclear SNP data identified the same four genetic clusters as the nuclear species tree (Figure 1B). The network showed extensive reticulation among the four clusters, yet also highlighted significant genetic distances between them (Figure 1B). Both *C. m. perspicillata* clusters connected *C. m. nigrifrons* and *C. m. melanops* (Figure 1B).

Population genetic structure

Principal component analysis of nuclear SNP data revealed four clearly separate genomic clusters in the Black-cheeked Gnateater: (1) one including all samples of *C. m. nigrifrons*, north of the São Francisco River; (2) one including all samples of *C. m. perspicillata* north of the Contas River; (3) one including all samples of *C. m. perspicillata* south of the Contas River; and (4) one including all samples of *C. m. melanops*, south of the Doce River (Figure 1C). The first principal component axis alone explained 34% of genotypic variance and discriminated the four groups, with both *C. m. perspicillata* clusters occupying intermediate positions between the more differentiated *C. m. nigrifrons* and *C. m. melanops* (Figure 1C). The second axis explained 10% of the genotypic variance and further discriminated the two *C. m. perspicillata* clusters from both *C. m. nigrifrons* and *C. m. melanops* (Figure 1C). Clustering algorithms produced broadly consistent results, indicating $k = 4$ as the statistically optimal number of clusters in the SNP data (Supplementary Figures S4 and S5).

Pairwise F_{ST} estimates indicated sizable differentiation among all four genetic clusters. Differentiation was greatest between *C. m. nigrifrons* and *C. m. melanops* ($F_{ST} = 0.46$) and between northern *C. m. perspicillata* and *C. m. melanops* ($F_{ST} = 0.39$). The smallest F_{ST} was between *C. m. nigrifrons* and northern *C. m. perspicillata* ($F_{ST} = 0.18$). The remaining pairwise F_{ST} estimates varied from 0.21 to 0.32. The number of fixed alleles between populations ranged from 0 to 22. We identified 22 fixed SNPs between *C. m. nigrifrons* and *C. m. melanops*, 2 between *C. m. nigrifrons* and southern *C. m. perspicillata*, 15 between *C. m. melanops* and northern *C. m. perspicillata*, 4 between *C. m. melanops* and southern *C. m. perspicillata*, and 2 between the two *C. m. perspicillata* clusters. The only comparison with no fixed SNPs was between *C. m. nigrifrons* and northern *C. m. perspicillata*. None of the four clusters had private alleles (i.e., alleles unique to that cluster).

The EEMS analysis showed areas of lower-than-expected gene flow relative to a null model of isolation-by-distance between *C. m. nigrifrons* and *C. m. perspicillata* and between *C. m. perspicillata* and *C. m. melanops*, but not between the two *C. m. perspicillata* clusters (Figure 2A). We observed a strong positive relationship between geographic and genetic distances as calculated in the EEMS analysis (Spearman's correlation: $\rho = 0.91$, $p < 0.0001$), with genetic distances increasing with geographic distance in a monotonic, non-linear fashion (Figure 2B). A quadratic polynomial model provided a good fit for this relationship ($R^2 = 0.85$, $p < 0.0001$; Figure 2B).

Mitochondrial haplotypes showed strong geographic structuring, with the three plumage-based subspecies and four nuclear genomic clusters showing discrete mitochondrial boundaries (Figure 4). The greatest differentiation was between *C. m. nigrifrons* and *C. m. melanops*, separated by 34–36 mutational steps (Figure 4). *Conopophaga m. perspicillata* was separated from *C. m. nigrifrons* and *C. m. melanops* by 20 and 12 mutational steps, respectively

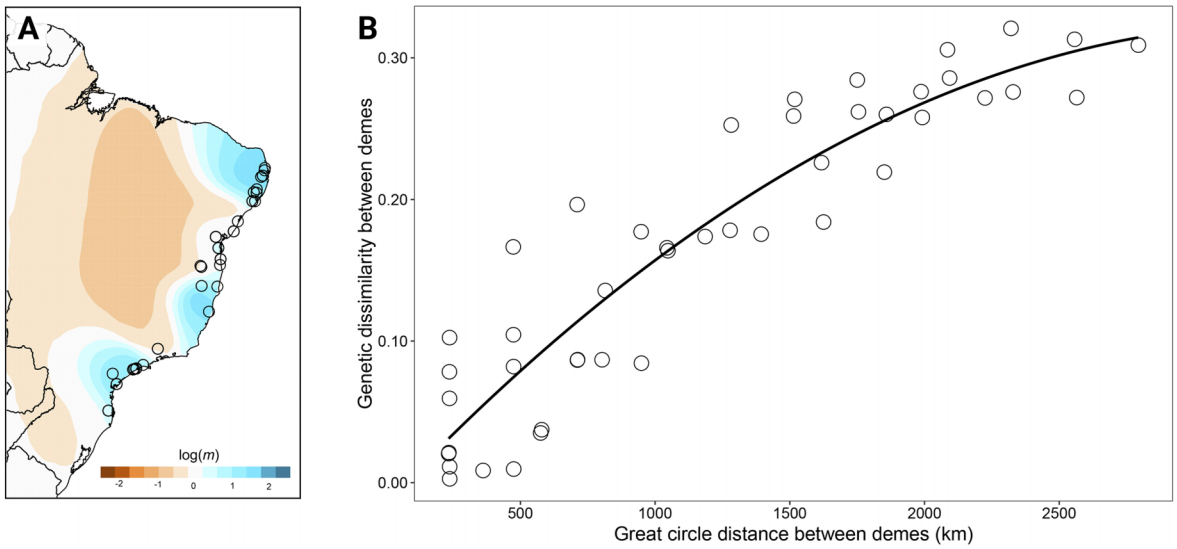

Figure 2. (A) EEMS showing areas of low and high gene flow. The effective migration rate (m) is a measure of gene flow relative to the expected value under a null model of isolation-by-distance. Orange shades indicate areas of lower gene flow than expected under isolation-by-distance, while blue shades indicate areas of higher-than-expected gene flow. Circles indicate sampling locations. (B) Positive relationship between geographic and genetic distances as calculated in the EEMS (quadratic polynomial model: $R^2 = 0.85$, $p < 0.0001$).

(Figure 4). Despite the lack of mitochondrial haplotype sharing between the two *C. m. perspicillata* nuclear genomic clusters, variation was greater within these clusters than between them (Figure 4). However, this absence of mitochondrial haplotype sharing across subspecies or nuclear clusters should be interpreted cautiously, as the mitochondrial DNA sample size (20 individuals from 12 different localities) was much smaller than that available for nuclear genes (45 individuals from 31 localities) owing to the poor quality of many off-target sequence reads from toepad samples. Uncorrected pairwise distances between *C. m. nigrifrons* and the other clusters ranged from 2.5% to 2.6% and were greatest between *C. m. nigrifrons* and *C. m. melanops*. *Conopophaga m. melanops* differed from both *C. m. perspicillata* clusters by 1.5%–1.6%, and the two *C. m. perspicillata* clusters differed from each other by 0.5%.

Genetic admixture

The sNMF analysis identified significant admixture between genetic clusters across all tested clustering scenarios. Cross-entropy values were smallest when using $\alpha = 10$, irrespective of the k value (Supplementary Figure S5). At $k = 2$, sNMF classified nearly all birds north of the Contas River as genetically pure individuals of one population and birds south of the Doce River as genetically pure individuals of the other population, with all birds between the Contas and Doce rivers highly admixed (Figure 1D). At $k = 3$, these highly admixed individuals were classified as a separate cluster, with admixture with both adjacent populations, particularly with birds between the São Francisco and Contas rivers (Figure 1D). At $k = 4$, sNMF identified admixture mainly between the two *C. m. perspicillata* clusters separated by the Contas River (Figure 1D). Most birds between the Contas and Doce rivers had highly admixed genotypes, with some shared ancestry with all other clusters (Figure 1D). In the northern *C. m. perspicillata* cluster, only the northernmost samples showed significant admixture with *C. m. nigrifrons* (Figure 1D). Across all three scenarios, almost all samples of *C. m. nigrifrons* and *C. m. melanops* showed no significant levels of admixture with other clusters.

A triangle plot based on the 22 fixed SNPs between *C. m. nigrifrons* and *C. m. melanops* showed most *C. m. perspicillata* individuals north of the Contas River as late-generation hybrids backcrossed with *C. m. nigrifrons*. The exceptions were two *C. m. perspicillata* individuals (samples 19 and 20) with interclass heterozygosity of zero, indicating no heterozygous loci derived from the two parentals for these SNPs. All individuals of *C. m. perspicillata* south of the Contas River exhibited heavily recombined genotypes (Figure 3A). Using a relaxed allele frequency difference threshold of 0.75 increased the number of ancestry-informative SNPs from 22 to 39. The resulting triangle plot closely resembled the previous one but showed all *C. m. perspicillata* individuals as having more heavily recombined genotypes (Figure 3B). Under this relaxed threshold, none of the *C. m. perspicillata* individuals had an interclass heterozygosity of zero, indicating that all have heterozygous loci from both parental populations. Importantly, none of the individuals identified as genetically admixed by sNMF were classified as early-generation hybrids in both triangle plots. Finally, plotting the heterozygosity of each genotyped sample against latitude revealed that heterozygosity peaks in the central populations, particularly around the Contas River (Figure 3C).

Geographic clines

The allele frequencies of 22 nuclear SNPs fixed between the northernmost and southernmost genomic clusters showed a sharp break at the Doce River and relatively smaller but abrupt breaks at the Contas and São Francisco rivers (Figure 4A). Male black forehead band width increased from south to north and showed a gradual transition near the Contas and Paraguaçu rivers (Figure 4B, Supplementary Figure S6A). There was broad overlap in trait values between the northernmost and southernmost populations, despite marked differences in the relative frequency of different forehead band widths (Figure 4B, Supplementary Figure

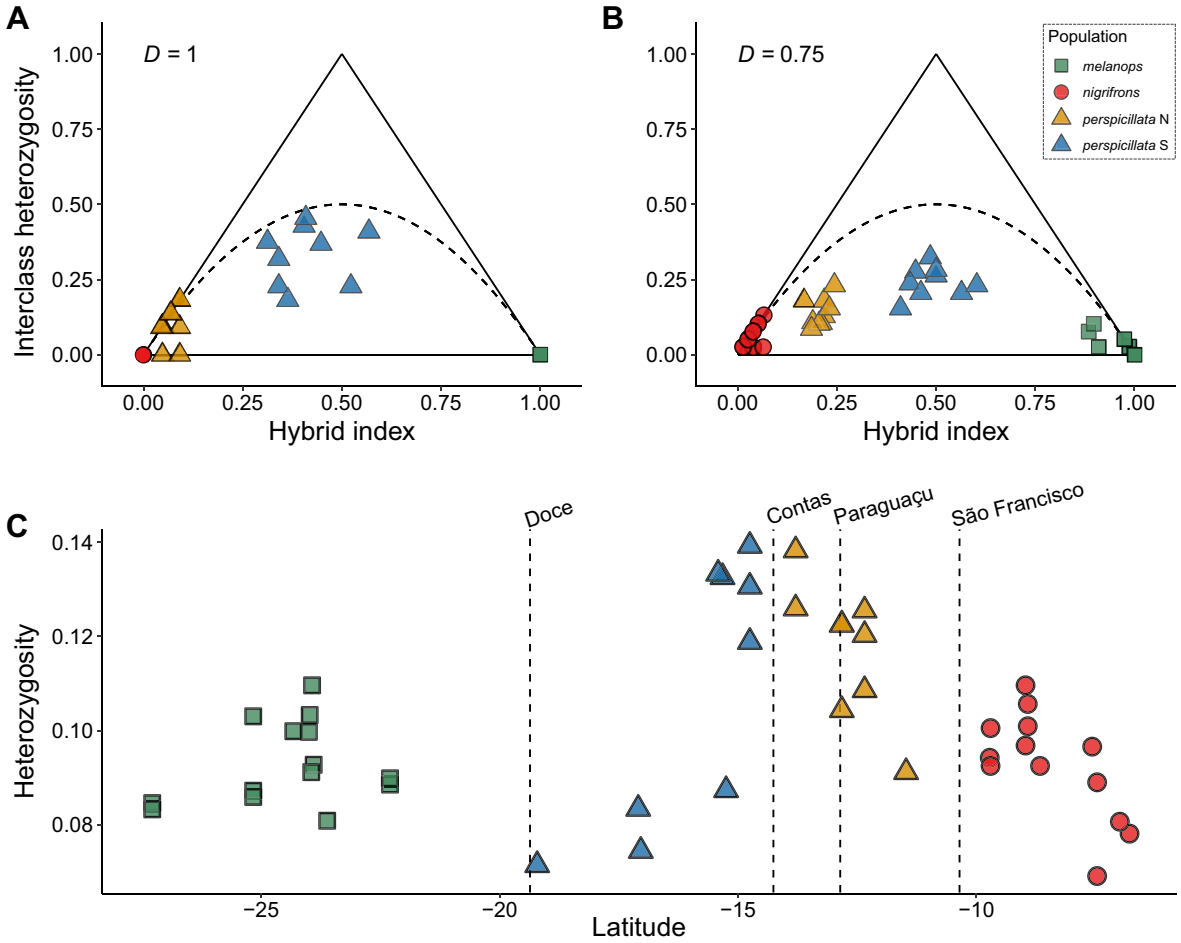

Figure 3. (A and B) Plots of interclass heterozygosity against hybrid indices calculated using two allele frequency difference thresholds ($D = 1$ and 0.75) suggest that the central populations of the Black-cheeked Gnateater have admixed genotypes resulting from historical hybridization between northern and southern populations. The left and right plots are based on 22 and 39 ancestry-informative nuclear SNPs, respectively. The triangular outline represents the possible plot space, and the dotted curve indicates the expected heterozygosity under Hardy–Weinberg equilibrium. Deviation from equilibrium in this case reflects population structure in the data, with subpopulations likely being in equilibrium. Recent hybrid generations typically exhibit elevated heterozygosity, and so they appear at the top apex (F_1 hybrids) or on the equilibrium curve in the center of the triangle (F_2 hybrids). The observed individuals fall below this curve, indicating historical rather than recent admixture. (C) Heterozygosity of each sample plotted against latitude, showing that heterozygosity peaks in the central populations (*perspicillata* N and S). Vertical lines indicate the geographic position of major rivers.

S6A). Although the substantial trait variability in populations with greater sample sizes suggests that the pattern of transition in this plumage trait could be fuzzier with greater sample sizes, our results suggest a transition in frequencies of this trait near the Contas and Paraguaçu rivers (Figure 4B). The frequency of male breast pattern scores appeared to change near the Paraguaçu River (Figure 4C, Supplementary Figure S6B). Although intermediate trait scores occurred throughout the species' range, there was a clear tendency for males south of the Paraguaçu River to have a clearly defined gray breast band whereas those north of this river typically had a white breast (Figure 4C, Supplementary Figure S6B). Male back color transitioned further south near the Contas River (Figure 4D, Supplementary Figure S6C). Although the two alternative character states scored for the male back color did not uniquely define any population (i.e., differences are not fixed), there was an abrupt change in the frequency of the two scores at the Contas River (Figure 4D, Supplementary Figure S6C). Female crown color showed a pronounced change at the Contas River (Figure 4E, Supplementary Figure S6D). Except for a single specimen south of the Contas River (specimen MZUSP 10,216), all females south of this river had either an orange–brown or dull brown crown, whereas all north of this river had either olive-brown or grayish-olive crowns. Finally, song pace showed an abrupt change between the São Francisco and Doce rivers (Figure 4F). Birds between these rivers exhibited significantly slower-paced songs (mean = 10 notes/s) than the remaining populations (mean = 16 notes/s). Birds north of the São Francisco River overlapped broadly in song pace with birds south of the Doce River (Figure 4F).

Discussion

The formation of a reticulate lineage

The patterns of genetic and phenotypic variation observed in the Black-cheeked Gnateater cannot be fully explained by isolation-by-distance or recent hybridization alone. While the positive correlation between geographic and genetic distances (Figure 2B) and range-wide clinal phenotypic variation (Figure 4) are consistent with isolation-by-distance, this

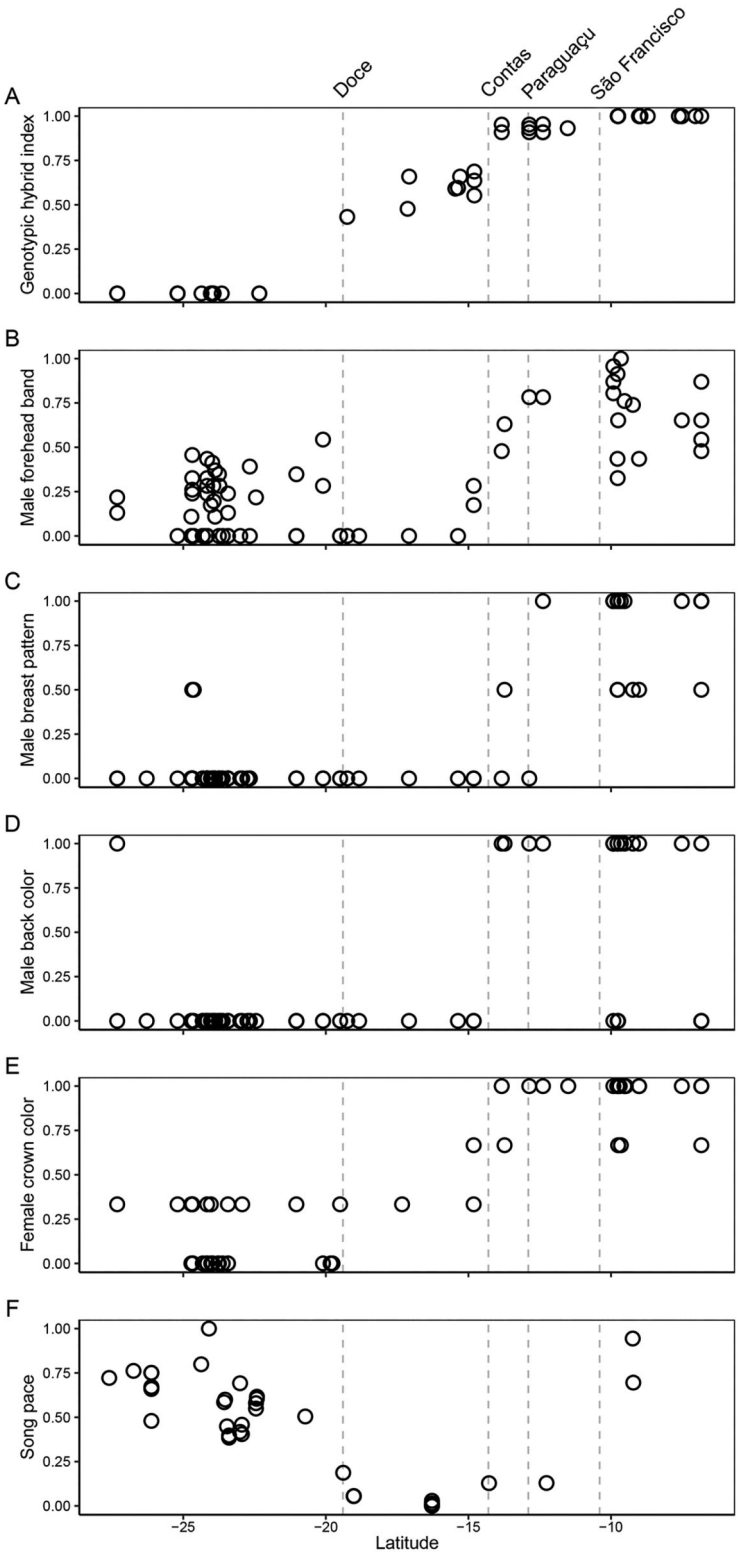

Figure 4. Latitudinal transitions in genotype and geographically varying phenotypic traits of the Black-cheeked Gnateater. Different variables were measured in different units and then scaled to range between 0 and 1 (details in Methods). Supplementary Figure S1 shows plumage traits.

model alone cannot explain the discrete genetic and phenotypic clusters (Figures 1, 4) or the marked geographic variation in heterozygosity (Figure 3C). Likewise, although the central populations have highly admixed genotypes (Figure 1D), the absence of early-generation hybrids (Figure 3A–B) indicates primarily historical admixture. Our dataset of 22–39 ancestry-informative SNPs provides high confidence in ruling out F_1 hybrids, but definitively excluding rare ongoing backcrossing may require >50 markers (Wiens et al., 2025). Consequently, the central populations could represent a re-

markably wide (~940 km) hybrid swarm that currently separates parentals geographically, preventing the formation of F_1s but allowing backcrossing at the margins. Countering this hypothesis, the central admixed populations exhibit significant nuclear (Figure 1B, C), mitochondrial (Figure 4), and phenotypic differentiation from the northern and southern lineages, including a distinct song pace (Figure 4F). Because gnateaters are suboscine passerines, which typically possess innate rather than learned vocalizations (Touchton et al., 2014), we assume that this variation in song pace reflects underlying genetic variation rather than plasticity or cultural transmission. Collectively, these findings suggest that these central admixed populations may comprise a reticulate lineage formed through past hybridization followed by geographic isolation.

The persistence of these admixed central populations in allopatry highlights the potential for post-hybridization vicariance to generate distinct lineages (Brelsford, 2011; James & Abbott, 2005). Hybrid populations exist along a continuum, ranging from transient hybrid swarms to stable lineages that may eventually evolve reproductive isolation from their parentals (Nolte & Tautz, 2010; Ottenburghs, 2018). This continuity may sometimes make it difficult to distinguish among distinct stages. This challenge is evident, for example, in the *Pipilo* towhees of the Trans-Mexican Volcanic Belt, where genomic data can be plausibly interpreted as isolation-by-distance, a tension zone, or incipient hybrid lineage formation depending on the framework applied (DeRaad et al., 2023). We observe a parallel complexity in the Black-cheeked Gnateater—the species shows isolation-by-distance (Figure 1C) and clinal plumage variation (Figure 4), yet the central admixed populations also form distinct genetic clusters and possess a distinct vocal phenotype (Figure 4F) characteristic of an independent lineage.

Our results suggest that the admixed central populations of the Black-cheeked Gnateater have persisted on their own evolutionary trajectory in allopatry for some time and have since accrued divergence from their parentals. Similar cases where divergence from parentals may have primarily occurred during a post-hybridization allopatric phase (e.g., Barrera-Guzmán et al., 2018; Brelsford et al., 2011; Hermansen et al., 2011; James & Abbott, 2005) are not widely considered hybrid speciation, as reproductive isolation may have evolved independently of hybridization (Long & Rieseberg, 2024; Schumer et al., 2014; Taylor & Larson, 2019). Although there is likely to be continued debate over whether hybrid swarms that later speciate in allopatry qualify as hybrid speciation (Feliner et al., 2017; Schumer et al., 2014), we agree that broad definitions risk erasing the mechanistic distinction between hybrid speciation and allopatric speciation.

A critical outstanding question is whether the distinct song pace of the admixed central populations (Figure 4F) represents a transgressive phenotype resulting from admixture that could contribute to reproductive isolation. Further genetic sampling across the Doce River could determine whether the vocally distinct populations are in geographic contact and, if so, assess reproductive isolation. If they are not in geographic contact, one could conduct field playback experiments to determine whether song differences could contribute to behavioral premating isolation.

Timing of divergence, refuges, and rivers

Mitochondrial phylogenies consistently recover three clades corresponding to the plumage-based subspecies of the Black-cheeked Gnateater (Supplementary Figure S3; Batalha-Filho et al., 2014). In contrast, phylogenetic analysis of genome-wide nuclear data identifies four distinct clades and groups the admixed central populations with different parental lineages (Supplementary Figure S2). This discordance likely reflects the greater susceptibility of the avian nuclear genome to introgression due to its biparental inheritance, larger effective population size, and widespread recombination, whereas the mitochondrial genome is typically non-recombining (Ottenburghs, 2022; Rheindt & Edwards, 2011). Thus, the mitochondrial phylogeny likely reflects the initial history of population divergence, whereas nuclear markers capture the species' history of extensive gene flow, grouping admixed lineages with the parental lineage with which they share the most alleles.

Mitochondrial divergence time estimates indicate that the three subspecies of the Black-cheeked Gnateater split during the mid-Pleistocene, between roughly 1.3 and 0.44 million years ago (Supplementary Figure S3; Batalha-Filho et al., 2014). This timing implicates Pleistocene climatic oscillations and the resulting contraction and expansion of forest refugia—rather than more ancient formation of rivers—as the primary drivers of geographic isolation and diversification. Pleistocene climatic oscillations played a prominent role in shaping present-day terrestrial lineage diversity patterns (Hewitt, 2000). These oscillations promoted both population subdivision, facilitating allopatric divergence, and geographic contact between differentiated populations, allowing for gene flow (Hewitt, 2004). Historical climate modelling identifies a large area of historical forest stability (i.e., refugium) between the São Francisco and Doce rivers in the central Atlantic Forest, and smaller areas to the north and south (Carnaval & Moritz, 2008; Carnaval et al., 2009). The geographic distribution of genomic clusters in the Black-cheeked Gnateater (Figure 1) shows notable spatial congruence with these predicted stability zones. The central admixed populations align closely with the large central refugium, while the northernmost cluster matches the northern refugium. The southernmost cluster encompasses the small southern refugium but extends far beyond it, suggesting a substantial southward range expansion as lowland forests expanded. Furthermore, the extensive size of the central refugium may explain the unequal admixture gradient in the central lineages (Figure 1D). It is likely that northern–central populations exchanged genes with the northern refugium, while distant southern–central populations interacted with the southern refugium, generating the current admixture gradient (Figure 1). Given the large size of the central refugium, it is likely that not enough time has passed since the admixture event for gene flow to homogenize ancestry proportions across the central populations.

Superimposed on this climatic legacy, rivers appear to have acted as secondary barriers that reinforced geographic isolation. Although the current courses of major Atlantic Forest rivers long predate the lineage diversification of the Black-cheeked Gnateater (Lundberg et al., 1998; Potter, 1997), genetic and phenotypic breaks consistently coincide with the São Francisco, Paraguaçu, Contas, and Doce rivers (Figures 1, 4). Because forest understory birds like

Conopophaga gnateaters are often poor dispersers, unable to fly over rivers only a few hundred meters wide (Naka et al., 2022), rivers can act as significant, albeit semipermeable, barriers to gene flow (Sotelo-Muñoz et al., 2020; Weir et al., 2024). Notably, the persistence of nuclear and mitochondrial genetic structure within the admixed central populations, despite geographic proximity of genomic clusters (Figures 1, 3), suggests a possible major role for the Contas River in maintaining this structure. Broadly, the spatial and temporal diversification of the Black-cheeked Gnateater aligns with biogeographic patterns observed across the Atlantic Forest. The role of Pleistocene refugia and riverine barriers in structuring genetic diversity is mirrored in several co-distributed avian lineages (Bocalini et al., 2021; Cabanne et al., 2008; d'Horta et al., 2011) and other vertebrate taxa (Peres et al., 2020), highlighting their broad impact on the regional biota.

Implications for taxonomy and conservation

Our results confirm that plumage variation in the Black-cheeked Gnateater is largely clinal (Figure 4B–E) and does not uniquely define the currently accepted subspecies. We also found discordance between phenotypic and genetic variation. In particular, our genetic analyses reveal that birds immediately south of the São Francisco River in northern Bahia differ markedly from those to the north both genetically (Figure 1) and vocally (Figure 4F), despite their similarity in plumage, which has traditionally led to the assignment of both populations to the threatened subspecies *C. m. nigrifrons* (Lima & Grantsau, 2005). This discordance indicates that plumage traits are relatively poor indicators of evolutionary lineages in this system compared with genomic structure and vocalizations.

Concluding remarks

Our results provide compelling evidence for a complex, reticulate evolutionary history in the Black-cheeked Gnateater, contrasting with earlier inferences of a simple bifurcating history based on limited genetic data (Batalha-Filho et al., 2014; Cabanne et al., 2016). This underscores that reticulate evolutionary histories are common (Mallet et al., 2016) but detectable only with extensive genomic and geographic sampling. Moreover, the Black-cheeked Gnateater may provide a valuable case study of how a lineage of hybrid origin can emerge and diverge, offering a window into the potential outcomes of reticulate evolution. Further genetic research with expanded geographic and genetic sampling is essential to deepen our understanding of this system and to test the hypotheses introduced here with more robust datasets. In particular, future genetic work could employ whole-genome sequencing to further characterize patterns of admixture, apply demographic modeling to explicitly test alternative diversification hypotheses, and estimate the species' phylogenetic history using regions of low recombination, where the correct species topology is less likely to be eroded by introgression (Burbrink et al., 2025). Further sampling across the Doce and Contas rivers is also particularly important to test the hypotheses discussed here.

Supplementary material

Supplementary material is available online at *Evolution*.

Data availability

Raw sequence data generated for this study are deposited in the NCBI Sequence Read Archive under accession number PRJNA1370955. All data and code necessary to reproduce the analyses are available at https://doi.org/10.5061/dryad.d2547d8cd.

Author contributions

R.D.L. conceived and designed the study, performed analyses, interpreted results, and wrote the manuscript. F.B. collected genetic data, processed raw sequence data, and performed species tree analysis. V.G. collected phenotypic data. E.N.O. and T.A.C. collected genetic data. J.D.W. and L.F.S. acquired funding and resources. V.Q.P. conceived the study, undertook fieldwork, collected genetic data, and acquired funding and resources. All authors read, edited, and approved the manuscript.

Funding

DNA extraction and sequencing were funded by Fundação de Amparo à Pesquisa do Estado de São Paulo (FAPESP grant no. 2017/23548-2 to LFS) and startup funds provided by Drexel University and the Academy of Natural Sciences of Drexel University to J.D.W. The authors also thank FAPESP, Conselho Nacional de Desenvolvimento Científico e Tecnológico (CNPq), Coordenação de Aperfeiçoamento de Pessoal de Nível Superior (CAPES), and the US National Science Foundation (NSF) for financial support (FAPESP grant no. 2021/10339-1 and CNPq grant no. 381507/2024-6 to R.D.L.; FAPESP grant no. 2020/16065-8 to F.B.; FAPESP grant no. 06/60300-4, CAPES Program PNPD, and CNPq grant no. 206689/2014-4 to V.Q.P.; NSF grants no. DEB-1503804 and DEB-1855812 to J.D.W.; and NSF grant no. DEB-2203228 to T.A.C. and J.D.W.).

Conflict of interest

The authors declare that they have no known competing financial interests or personal relationships that could have appeared to influence the work reported in this paper.

Acknowledgments

We are grateful to the numerous people who collected and preserved the genetic samples, study skins, and sound recordings used in this study, and the Field Museum of Natural History (FMNH), Laboratório de Genética e Evolução Molecular de Aves (LGEMA), Coleção de Aves Heretiano Zenaide (CAHZ), and Museu Paraense Emílio Goeldi (MPEG) for providing tissue samples. We also thank Michael G. Harvey, Glaucia Del-Rio, Scott Taylor, and five anonymous reviewers for comments on previous versions of the manuscript.

References

Abbott, R., Albach, D., Ansell, S., Arntzen, J. W., Baird, S. J. E., Bierne, N., Boughman, J., Brelsford, A., Buerkle, C. A., Buggs, R., Butlin, R. K., Dieckmann, U., Eroukhmanoff, F., Grill, A., Cahan, S. H., Hermansen, J. S., Hewitt, G., Hudson, A. G., Jiggins, C., … Zinner, D. (2013). Hybridization and speciation. *Journal of Evolutionary Bi-*

ology, *26*, 229–246. https://doi.org/10.1111/j.1420-9101.2012.02599.x

Barlow, A., Cahill, J. A., Hartmann, S., Theunert, C., Xenikoudakis, G., Fortes, G. G., Paijmans, J. L. A., Rabeder, G., Frischauf, C., Grandal-d'Anglade, A., García-Vázquez, A., Murtskhvaladze, M., Saarma, U., Anijalg, P., Skrbinšek, T., Bertorelle, G., Gasparian, B., Bar-Oz, G., Pinhasi, R., … Hofreiter, M. (2018). Partial genomic survival of cave bears in living brown bears. *Nature Ecology & Evolution*, *2*, 1563–1570. https://doi.org/10.1038/s41559-018-0654-8

Barrera-Guzmán, A. O., Aleixo, A., Shawkey, M. D., & Weir, J. T. (2018). Hybrid speciation leads to novel male secondary sexual ornamentation of an Amazonian bird. *Proceedings of the National Academy of Sciences*, *115*, E218–E225.

Batalha-Filho, H., Pessoa, R. O., Fabre, P.-H., Fjeldså, J., Irestedt, M., Ericson, P. G. P., Silveira, L. F., & Miyaki, C. Y. (2014). Phylogeny and historical biogeography of gnateaters (Passeriformes, Conopophagidae) in the South America forests. *Molecular Phylogenetics and Evolution*, *79*, 422–432. https://doi.org/10.1016/j.ympev.2014.06.025

Bertola, L. D., Quinn, L., Hanghøj, K., Garcia-Erill, G., Rasmussen, M. S., Balboa, R. F., Meisner, J., Bøggild, T., Wang, X., Lin, L., Nursyifa, C., Liu, X., Li, Z., Chege, M., Moodley, Y., Brüniche-Olsen, A., Kuja, J., Schubert, M., Agaba, M., … Heller, R. (2024). Giraffe lineages are shaped by major ancient admixture events. *Current Biology*, *34*, 1576–1586. https://doi.org/10.1016/j.cub.2024.02.051

Bocalini, F., Bolívar-Leguizamón, S. D., Silveira, L. F., & Bravo, G. A. (2021). Comparative phylogeographic and demographic analyses reveal a congruent pattern of sister relationships between bird populations of the northern and south-central Atlantic Forest. *Molecular Phylogenetics and Evolution*, *154*, 106973. https://doi.org/10.1016/j.ympev.2020.106973

Bolger, A. M., Lohse, M., & Usadel, B. (2014). Trimmomatic: a flexible trimmer for Illumina sequence data. *Bioinformatics*, *30*, 2114–2120. https://doi.org/10.1093/bioinformatics/btu170

Bouckaert, R., Heled, J., Kühnert, D., Vaughan, T., Wu, C.-H., Xie, D., Suchard, M. A., Rambaut, A., & Drummond, A. J. (2014). BEAST 2: A software platform for Bayesian evolutionary analysis. *Plos Computational Biology*, *10*, e1003537. https://doi.org/10.1371/journal.pcbi.1003537

Bouckaert, R. R., & Heled, J. (2014). DensiTree 2: seeing trees through the forest. bioRxiv.

Brelsford, A. (2011). Hybrid speciation in birds: allopatry more important than ecology? *Molecular Ecology*, *20*, 3705–3707. https://doi.org/10.1111/j.1365-294X.2011.05230.x

Brelsford, A., Milá, B., & Irwin, D. E. (2011). Hybrid origin of Audubon's warbler. *Molecular Ecology*, *20*, 2380–2389. https://doi.org/10.1111/j.1365-294X.2011.05055.x

Bryant, D., Bouckaert, R., Felsenstein, J., Rosenberg, N. A., & RoyChoudhury, A. (2012). Inferring species trees directly from biallelic genetic markers: bypassing gene trees in a full coalescent analysis. *Molecular Biology and Evolution*, *29*, 1917–1932. https://doi.org/10.1093/molbev/mss086

Bryant, D., & Huson, D. H. (2023). NeighborNet: improved algorithms and implementation. *Frontiers in Bioinformatics*, *3*, 1178600. https://doi.org/10.3389/fbinf.2023.1178600

Burbrink, F. T., DeBaun, D., Foley, N. M., & Murphy, W. J. (2025). Recombination-aware phylogenomics. *Trends in Ecology & Evolution*, *40*, 900–912. https://doi.org/10.1016/j.tree.2025.06.011

Cabanne, G., Dhorta, F., Sari, E., Santos, F., & Miyaki, C. (2008). Nuclear and mitochondrial phylogeography of the Atlantic forest endemic *Xiphorhynchus fuscus* (Aves: Dendrocolaptidae): biogeography and systematics implications. *Molecular Phylogenetics and Evolution*, *49*, 760–773. https://doi.org/10.1016/j.ympev.2008.09.013

Cabanne, G. S., Calderón, L., Trujillo Arias, N., Flores, P., Pessoa, R., d'Horta, F. M., & Miyaki, C. Y. (2016). Effects of Pleistocene climate changes on species ranges and evolutionary processes in the Neotropical Atlantic Forest. *Biological Journal of the Linnean Society*, *119*, 856–872. https://doi.org/10.1111/bij.12844

Carnaval, A. C., Hickerson, M. J., Haddad, C. F. B., Rodrigues, M. T., & Moritz, C. (2009). Stability predicts genetic diversity in the Brazilian Atlantic Forest hotspot. *Science (1979)*, *323*, 785–789.

Carnaval, A. C., & Moritz, C. (2008). Historical climate modelling predicts patterns of current biodiversity in the Brazilian Atlantic forest. *Journal of Biogeography*, *35*, 1187–1201. https://doi.org/10.1111/j.1365-2699.2007.01870.x

Charif, R. A., Waack, A. M., & Strickman, L. M. (2010). *Raven pro 1.4 user's manual*. Cornell Lab of Ornithology.

Clement, M., Posada, D., & Crandall, K. A. (2000). TCS: a computer program to estimate gene genealogies. *Molecular Ecology*, *9*, 1657–1659. https://doi.org/10.1046/j.1365-294x.2000.01020.x

Cui, R., Schumer, M., Kruesi, K., Walter, R., Andolfatto, P., & Rosenthal, G. G. (2013). Phylogenomics reveals extensive reticulate evolution in *Xiphophorus* fishes. *Evolution; International Journal of Organic Evolution*, *67*, 2166–2179. https://doi.org/10.1111/evo.12099

Darriba, D., Taboada, G. L., Doallo, R., & Posada, D. (2012). jModelTest 2: more models, new heuristics and parallel computing. *Nature Methods*, *9*, 772. https://doi.org/10.1038/nmeth.2109

Del-Rio, G., Rego, M. A., Whitney, B. M., Schunck, F., Silveira, L. F., Faircloth, B. C., & Brumfield, R. T. (2022). Displaced clines in an avian hybrid zone (Thamnophilidae: *Rhegmatorhina*) within an Amazonian interfluve. *Evolution; International Journal of Organic Evolution*, *76*, 455–475. https://doi.org/10.1111/evo.14377

DeRaad, D. A. (2022). SNPfiltR: An R package for interactive and reproducible SNP filtering. *Molecular Ecology Resources*, *22*, 2443–2453. https://doi.org/10.1111/1755-0998.13618

DeRaad, D. A., Applewhite, E. E., Tsai, W. L. E., Terrill, R. S., Kingston, S. E., Braun, M. J., & McCormack, J. E. (2023). Hybrid zone or hybrid lineage: a genomic reevaluation of Sibley's classic species conundrum in *Pipilo* towhees. *Evolution; International Journal of Organic Evolution*, *77*, 852–869. https://doi.org/10.1093/evolut/qpac068

d'Horta, F. M., Cabanne, G. S., Meyer, D., & Miyaki, C. Y. (2011). The genetic effects of Late Quaternary climatic changes over a tropical latitudinal gradient: diversification of an Atlantic Forest passerine. *Molecular Ecology*, *20*, 1923–1935.

Edelman, N. B., & Mallet, J. (2021). Prevalence and adaptive impact of introgression. *Annual Review of Genetics*, *55*, 265–283. https://doi.org/10.1146/annurev-genet-021821-020805

Faircloth, B. C. (2013). Illumiprocessor: a trimmomatic wrapper for parallel adapter and quality trimming. Available at: https://github.com/faircloth-lab/illumiprocessor (accessed August 2024).

Faircloth, B. C. (2016). PHYLUCE is a software package for the analysis of conserved genomic loci. *Bioinformatics*, *32*, 786–788. https://doi.org/10.1093/bioinformatics/btv646

Faircloth, B. C., McCormack, J. E., Crawford, N. G., Harvey, M. G., Brumfield, R. T., & Glenn, T. C. (2012). Ultraconserved elements anchor thousands of genetic markers spanning multiple evolutionary timescales. *Systematic Biology*, *61*, 717–726. https://doi.org/10.1093/sysbio/sys004

Feder, J. L., Egan, S. P., & Nosil, P. (2012). The genomics of speciation-with-gene-flow. *Trends in Genetics*, *28*, 342–350. https://doi.org/10.1016/j.tig.2012.03.009

Fitzpatrick, B. M. (2012). Estimating ancestry and heterozygosity of hybrids using molecular markers. *BMC Evolutionary Biology*, *12*, 1–14. https://doi.org/10.1186/1471-2148-12-131

Frichot, E., & François, O. (2015). LEA: An R package for landscape and ecological association studies. *Methods in Ecology and Evolution*, *6*, 925–929. https://doi.org/10.1111/2041-210X.12382

Frichot, E., Mathieu, F., Trouillon, T., Bouchard, G., & François, O. (2014). Fast and efficient estimation of individual ancestry coefficients. *Genetics*, *196*, 973–983. https://doi.org/10.1534/genetics.113.160572

Garrick, R. C., Benavides, E., Russello, M. A., Hyseni, C., Edwards, D. L., Gibbs, J. P., Tapia, W., Ciofi, C., & Caccone, A. (2014). Lineage fusion in Galápagos giant tortoises. *Molecular Ecology*, *23*, 5276–5290. https://doi.org/10.1111/mec.12919

Greeney, H. (2018). *Antpittas and gnateaters*. Helm.

Hahn, C., Bachmann, L., & Chevreux, B. (2013). Reconstructing mitochondrial genomes directly from genomic next-generation sequencing reads—a baiting and iterative mapping approach. *Nucleic Acids Research*, *41*, e129–e129. https://doi.org/10.1093/nar/gkt371

Harvey, M. G., Bravo, G. A., Claramunt, S., Cuervo, A. M., Derryberry, G. E., Battilana, J., Seeholzer, G. F., McKay, J. S., O'Meara, B. C., Faircloth, B. C., Edwards, S. V., Pérez-Emán, J., Moyle, R. G., Sheldon, F. H., Aleixo, A., Smith, B. T., Chesser, R. T., Silveira, L. F., Cracraft, J., … Derryberry, E. P. (2020). The evolution of a tropical biodiversity hotspot. *Science (1979)*, *370*, 1343–1348.

Harvey, M. G., Smith, B. T., Glenn, T. C., Faircloth, B. C., & Brumfield, R. T. (2016). Sequence capture versus restriction site associated DNA sequencing for shallow systematics. *Systematic Biology*, *65*, 910–924. https://doi.org/10.1093/sysbio/syw036

Hermansen, J. S., Sæther, S. A., Elgvin, T. O., Borge, T., Hjelle, E., & Sætre, G. -P. (2011). Hybrid speciation in sparrows I: phenotypic intermediacy, genetic admixture and barriers to gene flow. *Molecular Ecology*, *20*, 3812–3822. https://doi.org/10.1111/j.1365-294X.2011.05183.x

Hewitt, G. (2000). The genetic legacy of the Quaternary ice ages. *Nature*, *405*, 907–913. https://doi.org/10.1038/35016000

Hewitt, G. M. (2004). Genetic consequences of climatic oscillations in the Quaternary. *Philosophical Transactions of the Royal Society of London. Series B: Biological Sciences*, *359*, 183–195. https://doi.org/10.1098/rstb.2003.1388

Hurvich, C. M., & Tsai, C. L. (1989). Regression and time series model selection in small samples. *Biometrika*, *76*, 297–307. https://doi.org/10.1093/biomet/76.2.297

Huson, D. H., & Bryant, D. (2006). Application of phylogenetic networks in evolutionary studies. *Molecular Biology and Evolution*, *23*, 254–267. https://doi.org/10.1093/molbev/msj030

James, J. K., & Abbott, R. J. (2005). Recent, allopatric, homoploid hybrid speciation: the origin of *Senecio squalidus* (Asteraceae) in the British Isles from a hybrid zone on Mount Etna, *Sicily Evolution*, *59*, 2533–2547. https://doi.org/10.1111/j.0014-3820.2005.tb00967.x

Jombart, T. (2008). adegenet: a R package for the multivariate analysis of genetic markers. *Bioinformatics*, *24*, 1403–1405. https://doi.org/10.1093/bioinformatics/btn129

Jombart, T., Devillard, S., & Balloux, F. (2010). Discriminant analysis of principal components: a new method for the analysis of genetically structured populations. *BMC Genetics*, *11*, 94. https://doi.org/10.1186/1471-2156-11-94

Kearns, A. M., Restani, M., Szabo, I., Schrøder-Nielsen, A., Kim, J. A., Richardson, H. M., Marzluff, J. M., Fleischer, R. C., Johnsen, A., & Omland, K. E. (2018). Genomic evidence of speciation reversal in ravens. *Nature Communications*, *9*, 906. https://doi.org/10.1038/s41467-018-03294-w

Kearse, M., Moir, R., Wilson, A., Stones-Havas, S., Cheung, M., Sturrock, S., Buxton, S., Cooper, A., Markowitz, S., Duran, C., Thierer, T., Ashton, B., Meintjes, P., & Drummond, A. (2012). Geneious basic: an integrated and extendable desktop software platform for the organization and analysis of sequence data. *Bioinformatics*, *28*, 1647–1649. https://doi.org/10.1093/bioinformatics/bts199

Knaus, B. J., & Grünwald, N. J. (2017). vcfR: a package to manipulate and visualize variant call format data in R. *Molecular Ecology Resources*, *17*, 44–53. https://doi.org/10.1111/1755-0998.12549

Kuhlwilm, M., Han, S., Sousa, V. C., Excoffier, L., & Marques-Bonet, T. (2019). Ancient admixture from an extinct ape lineage into bonobos. *Nature Ecology & Evolution*, *3*, 957–965. https://doi.org/10.1038/s41559-019-0881-7

Leigh, J. W., & Bryant, D. (2015). POPART: full-feature software for haplotype network construction. *Methods in Ecology and Evolution*, *6*, 1110–1116. https://doi.org/10.1111/2041-210X.12410

Li, H., & Durbin, R. (2010). Fast and accurate long-read alignment with Burrows–Wheeler transform. *Bioinformatics*, *26*, 589–595. https://doi.org/10.1093/bioinformatics/btp698

Li, H., Handsaker, B., Wysoker, A., Fennell, T., Ruan, J., Homer, N., Marth, G., Abecasis, G., & Durbin, R. (2009). The Sequence Alignment/Map format and SAMtools. *Bioinformatics*, *25*, 2078–2079. https://doi.org/10.1093/bioinformatics/btp352

Lima, P. C., & Grantsau, R. (2005). *Conopophaga melanops nigrifrons* Pinto, 1943–nova ocorrência para a Bahia. *Atualidades Ornitológicas*, *127*, *5*.

Linck, E., & Battey, C. J. (2019). Minor allele frequency thresholds strongly affect population structure inference with genomic data sets. *Molecular Ecology Resources*, *19*, 639–647. https://doi.org/10.1111/1755-0998.12995

Long, Z., & Rieseberg, L. H. (2024). Documenting homoploid hybrid speciation. *Molecular Ecology*, *34*, e17412.

Lopes, F., Oliveira, L. R., Beux, Y., Kessler, A., Cárdenas-Alayza, S., Majluf, P., Páez-Rosas, D., Chaves, J., Crespo, E., Brownell, R. L., Baylis, A. M. M., Sepúlveda, M., Franco-Trecu, V., Loch, C., Robertson, B. C., Peart, C. R., Wolf, J. B. W., & Bonatto, S. L. (2023). Genomic evidence for homoploid hybrid speciation in a marine mammal apex predator. *Science Advances*, *9*, eadf6601. https://doi.org/10.1126/sciadv.adf6601

Lundberg, J. G., Marshall, L. G., Guerrero, J., Horton, B., Malabarba, M. C. S. L., & Wesselingh, F. (1998). The stage for neotropical fish diversification a history of tropical South American rivers. In L. R. Malabarba, R. E. Reis, R. P. Vari, Z. M. S. Lucena, & C. A. S. Lucena (Eds.), *Phylogeny and classification of neotropical fishes* (pp. 13–48). Edipucrs.

Mallet, J., Besansky, N., & Hahn, M. W. (2016). How reticulated are species? *BioEssays*, *38*, 140–149. https://doi.org/10.1002/bies.201500149

McCallum, Q., Askelson, K., Fogarty, F. F., Natola, L., Nikelski, E., Huang, A., & Irwin, D. (2024). Pronounced differentiation on the Z chromosome and parts of the autosomes in crowned sparrows contrasts with mitochondrial paraphyly: implications for speciation. *Journal of Evolutionary Biology*, *37*, 171–188. https://doi.org/10.1093/jeb/voae004

McKenna, A., Hanna, M., Banks, E., Sivachenko, A., Cibulskis, K., Kernytsky, A., Garimella, K., Altshuler, D., Gabriel, S., Daly, M., & DePristo, M. A. (2010). The Genome Analysis Toolkit: A MapReduce framework for analyzing next-generation DNA sequencing data. *Genome Research*, *20*, 1297–1303. https://doi.org/10.1101/gr.107524.110

Musher, L. J., Del-Rio, G., Marcondes, R. S., Brumfield, R. T., Bravo, G. A., & Thom, G. (2024). Geogenomic predictors of genetree heterogeneity explain phylogeographic and introgression history: a case study in an Amazonian bird (*Thamnophilus aethiops*). *Systematic Biology*, *73*, 36–52. https://doi.org/10.1093/sysbio/syad061

Musher, L. J., Giakoumis, M., Albert, J., Del-Rio, G., Rego, M., Thom, G., Aleixo, A., Ribas, C. C., Brumfield, R. T., Smith, B. T., & Cracraft, J. (2022). River network rearrangements promote speciation in lowland Amazonian birds. *Science Advances*, *8*, eabn1099. https://doi.org/10.1126/sciadv.abn1099

Nabholz, B., Lanfear, R., & Fuchs, J. (2016). Body mass-corrected molecular rate for bird mitochondrial DNA. *Molecular Ecology*, *25*, 4438–4449. https://doi.org/10.1111/mec.13780

Naka, L. N., Costa, B. M. S., Lima, G. R., & Claramunt, S. (2022). Riverine barriers as obstacles to dispersal in Amazonian birds. *Frontiers in Ecology and Evolution*, *10*, 846975. https://doi.org/10.3389/fevo.2022.846975

Nei, M. (1972). Genetic distance between populations. *American Naturalist*, *106*, 283–292. https://doi.org/10.1086/282771

Nieto Feliner, G., Álvarez, I., Fuertes-Aguilar, J., Heuertz, M., Marques, I., Moharrek, F., Piñeiro, R., Riina, R., Rosselló, J. A., Soltis, P. S., & Villa-Machío, I. (2017). Is homoploid hybrid speciation that rare? An empiricist's view. *Heredity (Edinb)*, *118*, 513–516. https://doi.org/10.1038/hdy.2017.7

Nolte, A. W., & Tautz, D. (2010). Understanding the onset of hybrid speciation. *Trends in Genetics*, *26*, 54–58. https://doi.org/10.1016/j.tig.2009.12.001

Ottenburghs, J. (2018). Exploring the hybrid speciation continuum in birds. *Ecology & Evolution*, *8*, 13027–13034. https://doi.org/10.1002/ece3.4558

Ottenburghs, J. (2022). Avian introgression patterns are consistent with Haldane's rule. *Journal of Heredity*, *113*, 363–370. https://doi.org/10.1093/jhered/esac005

Pembleton, L. W., Cogan, N. O. I., & Forster, J. W. (2013). StAMPP: an R package for calculation of genetic differentiation and structure of mixed-ploidy level populations. *Molecular Ecology Resources*, *13*, 946–952. https://doi.org/10.1111/1755-0998.12129

Peñalba, J. V., Runemark, A., Meier, J. I., Singh, P., Wogan, G. O. U., Sánchez-Guillén, R., Mallet, J., Rometsch, S. J., Menon, M., Seehausen, O., Kulmuni, J., & Pereira, R. J. (2024). The role of hybridization in species formation and persistence. *Cold Spring Harbor Perspectives in Biology*, *16*: a041445.

Peres, E. A., Pinto-da-Rocha, R., Lohmann, L. G., Michelangeli, F. A., Miyaki, C. Y., & Carnaval, A. C. (2020). Patterns of species and lineage diversity in the Atlantic rainforest of Brazil. In V. Rull, & A. C. Carnaval (Eds.), *Neotropical diversification: patterns and processes* (pp. 415–447). Springer.

Petkova, D., Novembre, J., & Stephens, M. (2016). Visualizing spatial population structure with estimated effective migration surfaces. *Nature Genetics*, *48*, 94–100. https://doi.org/10.1038/ng.3464

Potter, P. E. (1997). The Mesozoic and Cenozoic paleodrainage of South America: a natural history. *Journal of South American Earth Sciences*, *10*, 331–344. https://doi.org/10.1016/S0895-9811(97)00031-X

Price, T. (2008). *Speciation in birds*. Roberts & Company.

Prjibelski, A., Antipov, D., Meleshko, D., Lapidus, A., & Korobeynikov, A. (2020). Using SPAdes de novo assembler. *Current Protocols in Bioinformatics*, *70*, e102. https://doi.org/10.1002/cpbi.102

Pulido-Santacruz, P., Aleixo, A., & Weir, J. T. (2020). Genomic data reveal a protracted window of introgression during the diversification of a neotropical woodcreeper radiation. *Evolution; International Journal of Organic Evolution*, *74*, 842–858. https://doi.org/10.1111/evo.13902

Rambaut, A., Drummond, A. J., Xie, D., Baele, G., & Suchard, M. A. (2018). Posterior summarization in Bayesian phylogenetics using Tracer 1.7. *Systematic Biology*, *67*, 901–904. https://doi.org/10.1093/sysbio/syy032

Rheindt, F. E., & Edwards, S. V. (2011). Genetic introgression: an integral but neglected component of speciation in birds. *The Auk*, *128*, 620–632. https://doi.org/10.1525/auk.2011.128.4.620

Ribas, C. C., Aleixo, A., Gubili, C., d'Horta, F. M., Brumfield, R. T., & Cracraft, J. (2018). Biogeography and diversification of *Rhegmatorhina* (Aves: Thamnophilidae): Implications for the evolution of Amazonian landscapes during the Quaternary. *Journal of Biogeography*, *45*, 917–928. https://doi.org/10.1111/jbi.13169

Schliep, K., Potts, A. J., Morrison, D. A., & Grimm, G. W. (2017). Intertwining phylogenetic trees and networks. *Methods in Ecology and Evolution*, *8*, 1212–1220. https://doi.org/10.1111/2041-210X.12760

Schliep, K. P. (2011). phangorn: phylogenetic analysis in R. *Bioinformatics*, *27*, 592–593. https://doi.org/10.1093/bioinformatics/btq706

Schultz, E. D., Pérez-Emán, J., Aleixo, A., Miyaki, C. Y., Brumfield, R. T., Cracraft, J., & Ribas, C. C. (2019). Diversification history in the *Dendrocincla fuliginosa* complex (Aves: Dendrocolaptidae): Insights from broad geographic sampling. *Molecular Phylogenetics and Evolution*, *140*, 106581. https://doi.org/10.1016/j.ympev.2019.106581

Schumer, M., Rosenthal, G. G., & Andolfatto, P. (2014). How common is homoploid hybrid speciation? *Evolution; International Journal of Organic Evolution*, *68*, 1553–1560. https://doi.org/10.1111/evo.12399 .

Seehausen, O. (2004). Hybridization and adaptive radiation. *Trends in Ecology & Evolution*, *19*, 198–207. https://doi.org/10.1016/j.tree.2004.01.003

Singhal, S., Derryberry, G. E., Bravo, G. A., Derryberry, E. P., Brumfield, R. T., & Harvey, M. G. (2021). The dynamics of introgression across an avian radiation. *Evolution Letters*, *5*, 568–581. https://doi.org/10.1002/evl3.256

Sotelo-Muñoz, M., Maldonado-Coelho, M., Svensson-Coelho, M., dos Santos, S. S., & Miyaki, C. Y. (2020). Vicariance, dispersal, extinction and hybridization underlie the evolutionary history of Atlantic forest fire-eye antbirds (Aves: Thamnophilidae). *Molecular Phylogenetics and Evolution*, *148*, 106820. https://doi.org/10.1016/j.ympev.2020.106820

Taylor, E. B., Boughman, J. W., Groenenboom, M., Sniatynski, M., Schluter, D., & Gow, J. L. (2006). Speciation in reverse: morphological and genetic evidence of the collapse of a three-spined stickleback (*Gasterosteus aculeatus*) species pair. *Molecular Ecology*, *15*, 343–355. https://doi.org/10.1111/j.1365-294X.2005.02794.x

Taylor, R. S., Bramwell, A. C., Clemente-Carvalho, R., Cairns, N. A., Bonier, F., Dares, K., & Lougheed, S. C. (2021). Cytonuclear discordance in the crowned-sparrows, *Zonotrichia atricapilla* and *Zonotrichia leucophrys*. *Molecular Phylogenetics and Evolution*, *162*, 107216. https://doi.org/10.1016/j.ympev.2021.107216

Taylor, S. A., & Larson, E. L. (2019). Insights from genomes into the evolutionary importance and prevalence of hybridization in nature. *Nature Ecology & Evolution*, *3*, 170–177. https://doi.org/10.1038/s41559-018-0777-y

Thia, J. A. (2023). Guidelines for standardizing the application of discriminant analysis of principal components to genotype data. *Molecular Ecology Resources*, *23*, 523–538. https://doi.org/10.1111/1755-0998.13706

Thom, G., & Aleixo, A. (2015). Cryptic speciation in the white-shouldered antshrike (*Thamnophilus aethiops*, Aves—Thamnophilidae): The tale of a transcontinental radiation across rivers in lowland Amazonia and the northeastern Atlantic Forest. *Molecular Phylogenetics and Evolution*, *82*, 95–110. https://doi.org/10.1016/j.ympev.2014.09.023

Touchton, J. M., Seddon, N., & Tobias, J. A. (2014). Captive rearing experiments confirm song development without learning in a tracheophone suboscine bird. *PLoS One*, *9*, e95746. https://doi.org/10.1371/journal.pone.0095746 .

Uy, J. A. C., Irwin, D. E., & Webster, M. S. (2018). Behavioral isolation and incipient speciation in birds. *Annual Review of Ecology, Evolution, and Systematics*, *49*, 1–24. https://doi.org/10.1146/annurev-ecolsys-110617-062646

Weckstein, J. D., Zink, R. M., Blackwell-Rago, R. C., & Nelson, D. A. (2001). Anomalous variation in mitochondrial genomes of white-crowned (*Zonotrichia leucophrys*) and golden-crowned (*Z. atricapilla*) sparrows: Pseudogenes, hybridization, or incomplete lineage sorting? *The Auk*, *118*, 231–236. https://doi.org/10.1093/auk/118.1.231

Weir, B. S., & Cockerham, C. C. (1984). Estimating *F*-statistics for the analysis of population structure. *Evolution; International Journal of Organic Evolution*, *38*, 1358–1370.

Weir, J. T., Aleixo, A., & Pulido-Santacruz, P. (2024). Amazonian rivers are leaky barriers to gene flow in forest understory birds. *Proceedings of the Royal Society B: Biological Sciences*, *291*, 20240795. https://doi.org/10.1098/rspb.2024.0795

Whitney, B. M. (2003). Family Conopophagidae (gnateaters). In J. del Hoyo, A. Elliot, & D. A. Christie (Eds.), *Handbook of the birds of the world* (pp. 732–748). Lynx Edicions.

Wiens, B. J., DeCicco, L. H., & Colella, J. P. (2025). *triangulaR*: an R package for identifying AIMs and building triangle plots using SNP data from hybrid zones. *Heredity (Edinb)*, *134*, 251–262. https://doi.org/10.1038/s41437-025-00760-2

Willing, E.-M., Dreyer, C., & van Oosterhout, C. (2012). Estimates of genetic differentiation measured by F_{ST} do not necessarily require large sample sizes when using many SNP markers. *PLoS One*, *7*, e42649. https://doi.org/10.1371/journal.pone.0042649 .

Wu, H., Wang, Z., Zhang, Y., Frantz, L., Roos, C., Irwin, D. M., Zhang, C., Liu, X., Wu, D., Huang, S., Gu, T., Liu, J., & Yu, L. (2023). Hybrid origin of a primate, the gray snub-nosed monkey. *Science (1979)*, *380*, eabl4997.

Yi, X., & Latch, E. K. (2022). Nonrandom missing data can bias Principal Component Analysis inference of population genetic structure. *Molecular Ecology Resources*, *22*, 602–611. https://doi.org/10.1111/1755-0998.13498

Yu, G., Smith, D. K., Zhu, H., Guan, Y., & Lam, T. T. (2017). ggtree: an r package for visualization and annotation of phylogenetic trees with their covariates and other associated data. *Methods in Ecology and Evolution*, *8*, 28–36. https://doi.org/10.1111/2041-210X.12628

Received June 18, 2025; revisions received March 30, 2026; accepted April 21, 2026
Associate Editor: Scott Taylor; Handling Editor: Jason Wolf